RSC Advances

PAPER

View Article Online
View Journal | View Issue

Cite this: *RSC Adv.*, 2024, **14**, 36132

Facile fabrication of g-C_3N_4/Bi_2S_3 coated melamine foam for oil/water separation applications†

Swathi A. C. and Maneesh Chandran *

Received 30th September 2024
Accepted 6th November 2024

DOI: 10.1039/d4ra07030e

rsc.li/rsc-advances

Regular occurrences of oil leaks are recognized as a significant contributor to water pollution, resulting in substantial environmental and ecological challenges, as well as posing potential for fires and explosions. Therefore, it is imperative to create a cost-effective and exceptionally effective absorbent material for separating oil and water. Hydrophobic, foam-like materials have garnered considerable attention as potential absorbers for addressing oil spills and recovering oil from water sources. In this experimental study, simple, low-cost, environmentally friendly, highly hydrophobic, and super oleophilic g-C_3N_4/Bi_2S_3 nanocomposite-coated melamine foam was introduced for oily wastewater treatment. The g-C_3N_4 and Bi_2S_3 were synthesized by thermal decomposition and hydrothermal methods, and the g-C_3N_4/Bi_2S_3 composite-coated foam was prepared by a simple dip-coated method. The g-C_3N_4/Bi_2S_3 composite-coated melamine foam shows excellent absorption capacity, and it can absorb various oils and solvents and separate different oils and solvents from water. Hence, the developed g-C_3N_4/Bi_2S_3 foam absorbent has excellent potential in oil/water separation applications.

Introduction

The frequent oil leakage from industries is considered a main source of water pollution. This has caused severe environmental and ecological problems, creating potential risks of fire and explosion in recent years.[1–3] Conventional methods like *in situ* burning and filtration are more time-consuming and expensive, so there is an urgent need to develop a low-cost, highly efficient absorbent material for oily wastewater treatment.[4] An ideal material for this purpose must have high absorption capacity and better recyclability. Therefore, the studies on the controlled synthesis of carbon nanocomposite-coated absorbent materials are of great interest and are actively being pursued.

Over the past few years, foams have received considerable attention for their potential as oil-absorbent materials due to their unique characteristics compared to other absorbents, such as aerogels, zeolites, synthetic polymers, and natural materials.[5,6] For example, commercial melamine foam is low-cost with low density, high porosity, excellent elasticity, and environmental friendliness. Nevertheless, pure melamine foam is super hydrophilic ($\theta = 0°$) and super oleophilic ($\theta = 0°$), and hence, chemical modifications are necessary for oil/water separation applications.[7] It has been reported that absorber coatings made from foams exhibit superior absorption rates, low density, ease of preparation, low cost, and high reusability. There are various sorbent materials with micro/nano particles that have been reported. In 2019, Meenakshi Talukdar, *et.al.* developed an innovative, surface-engineered sorbent material with advanced properties for the efficient magnetic separation of oil from oily water mixtures.[8] Further, De Liu *et al.* fabricated multi-walled carbon nanotubes loaded superhydrophobic polyurethane sponge for oil/water separation.[9] However, the practical applications are hindered due to the recovery process of sorbent material, high cost and complicated synthesis procedure of nanoparticles. Membrane-based absorbers for oil/water separation also exhibit high selectivity and absorption efficiency. However, in membrane-based filters, the oil/water mixture has to be poured onto the surface for the separation to happen, which may be difficult for large-scale separation.[10,11]

In the present work, composite containing graphitic carbon nitride (g-C_3N_4) and bismuth sulfide (Bi_2S_3) was introduced into melamine foam for effective oil/water separation for the first time. g-C_3N_4 shows exceptional thermal and chemical stability, rendering it highly suitable for use in extreme harsh environments where oil/water separation is necessary, such as in the treatment of industrial effluents or the remediation of oil spills.[12,13] Also, g-C_3N_4 based foam exhibits a self-cleaning mechanism, which consequently minimizes maintenance demands and reduces operational costs.[14–16] In addition to this, the Bi_2S_3 also shows properties such as tunable surface wettability, high surface area, selectivity, and stability, and unique physicochemical characteristics in both acidic and alkaline environments.[17,18] So, the combination of Bi_2S_3 and g-C_3N_4 is used to enable efficient oil-water separation in practical applications. The g-C_3N_4/Bi_2S_3 nanocomposite absorber foams are

National Institute of Technology Calicut, Kerala, 673601, India. E-mail: maneesh@nitc.ac.in

† Electronic supplementary information (ESI) available. See DOI: https://doi.org/10.1039/d4ra07030e

selected based on the ease of synthesis, cost-effectiveness, good selectivity, and high absorption capacity for large-scale applications. A simple and affordable one-step hydrothermal method was used for the synthesis of g-C_3N_4/Bi_2S_3 nanocomposite, and a simple dip coating method was utilized for the preparation of g-C_3N_4/Bi_2S_3 foam. The g-C_3N_4/Bi_2S_3 composite-coated melamine foam showed outstanding superhydrophobic and superoleophilic surface characteristics. It also showed sufficient absorption capacity and could be reused efficiently.

Experimental

Materials

The following commercially available materials were used for the present work: melamine (Sigma-Aldrich, 99%), thiourea (Sigma-Aldrich, 99%), bismuth nitrate pentahydrate (99.99%), furfuryl alcohol (98%), ethanol, hydrochloric acid, tris buffer (tri(hydroxymethyl)aminomethane) (Thermo Fisher Scientific, 99%), dopamine hydrochloride (98%), 1-octadecanethiol (97%), and deionized (DI) water. Commercially available olive oil, engine oil, diesel, acetone, chloroform, pump oil, ethanol, methanol, toluene, and crude oil were used for the oil absorption studies, and commercially available melamine foam was used for the preparation of g-C_3N_4/Bi_2S_3 foam oil absorbent.

Preparation of g-C_3N_4/Bi_2S_3

Initially, the g-C_3N_4 was synthesized using melamine precursor. 5 g of melamine was calcinated at 550 °C in a muffle furnace [LT 9, Nabertherm] for 2 h at a heating rate of 10 °C min^{-1} to get g-C_3N_4. After cooling down to room temperature, the yellow product was collected and ground into a fine powder.

A one-step hydrothermal method was employed to synthesize the g-C_3N_4/Bi_2S_3 binary nanocomposite. Initially, 5 ml of furfuryl alcohol was mixed with 60 ml of DI water for 1 h, and 250 mg of thiourea, 610 mg of bismuth nitrate pentahydrate ($Bi(NO_3)_3 \cdot 5H_2O$), and an appropriate amount of g-C_3N_4 (0 mg, 100 mg, 200 mg, 250 mg, 300 mg 500 mg, 750 mg, and 1000 mg) were added to the above solution and stirred for 1 h. This suspension was transferred into a Teflon-lined autoclave assembly and heated in an oven at 180 °C for 12 h. Subsequently, the product was centrifuged, rinsed several times with DI water and ethanol, and dried at 60 °C for 12 h. The final product was again treated with 0.2 M HCl solution for 6 h, and dried at 80 °C for 8 h to obtain the g-C_3N_4/Bi_2S_3 binary nanocomposite (see ESI Section† for detail).

Preparation of g-C_3N_4/Bi_2S_3 foam

Preparation of g-C_3N_4/Bi_2S_3 foam is schematically shown in Fig. 1. Initially, commercially available melamine foam was cut into 1 × 1 × 1 cm^3 dimensions, cleaned in DI water and acetone by ultrasonication for 15 min, and dried at a temperature of 60 °C for 5 h. The g-C_3N_4/Bi_2S_3 foam was prepared using the dip coating method. At first, g-C_3N_4/Bi_2S_3 binary composite with various ratios were dispersed into 50 ml DI water by sonication for 20 min. Afterward, 100 mg dopamine hydrochloride, 50 mg tris buffer, and cleaned melamine foam were added to the above solution and stirred at 400 rpm for 12 h at 40 °C. Secondly, the product was collected and washed several times with DI water, and dried at a temperature of 60 °C for 12 h. Finally, the product was dipped into octadecanthiol (200 mg) and ethanol (100 ml) dispersion for 8 h under a water bath temperature of 50 °C and dried at 60 °C for 6 h. The dopamine hydrochloride and octadecanethiol collectively served as binding agents to ensure robust composite adhesion and surface stability.

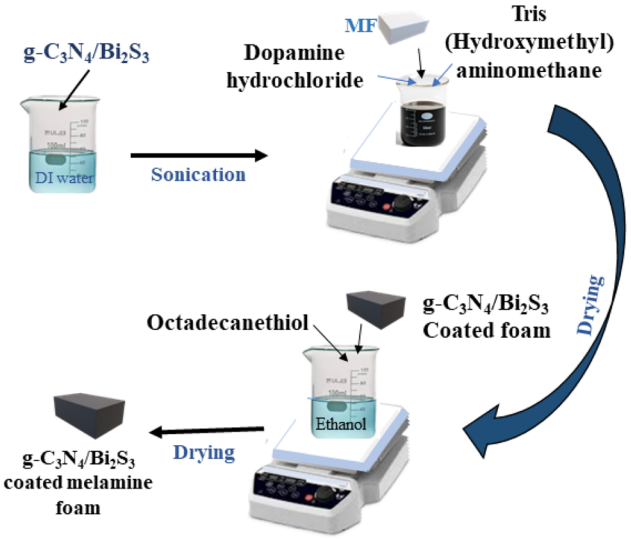

Fig. 1 Schematic diagram for the preparation of g-C_3N_4/Bi_2S_3 coated melamine foam.

Characterization

The structure of the synthesized samples was characterized using an X-ray diffractometer (XRD: Rigaku SmartLab SE). The morphology of pure melamine foam and g-C_3N_4/Bi_2S_3 coated melamine foam was imaged using scanning electron microscopy (FESEM: Hitachi SU6600). The surface composition of the prepared samples was analyzed using an X-ray photoelectron spectrometer (XPS: PHI5000 Version probe III). The water contact angle (WCA) of the sample was measured using a contact angle measuring instrument (Holmarc: HO-IAD-CAM-01A). The thermal analysis of samples was performed using thermogravimetric (TGA Q50) instrument and Fourier transform infrared spectra (FTIR) of synthesized samples were obtained using Perkin Elmer-spectrum two FTIR spectrometer.

Results and discussion

XRD analysis

The XRD patterns of the synthesized g-C_3N_4, Bi_2S_3, and g-C_3N_4/Bi_2S_3 nanocomposites are shown in Fig. 2. The diffraction peak of g-C_3N_4 (100), observed at 13°, corresponds to the planar structure of the tri-*s*-triazine unit. In addition, the prominent diffraction peak at 27.6° is associated with the graphite-like interlayer stacking peak (002) of g-C_3N_4.[19–21] The XRD pattern of g-C_3N_4/Bi_2S_3 exhibited peaks corresponding to both g-C_3N_4 and Bi_2S_3 (ICDD Card No. 03-065-3884), indicating successful formation of the composites. Fig. S1 (see ESI document)† shows

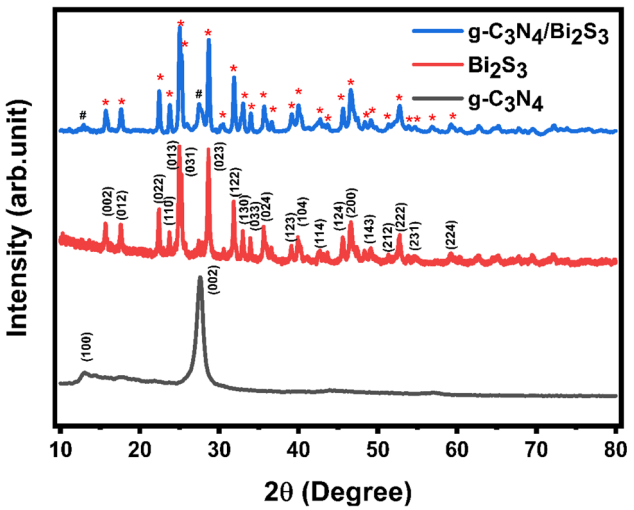

Fig. 2 XRD patterns of synthesized g-C_3N_4, Bi_2S_3, and g-C_3N_4/Bi_2S_3 nanocomposite.

the XRD pattern of pure melamine foam and g-C_3N_4/Bi_2S_3 foam, which confirmed the successful coating of g-C_3N_4/Bi_2S_3 on the melamine skeleton.

Morphological analysis

The SEM images of commercially available pure melamine foam and the prepared g-C_3N_4/Bi_2S_3 foam samples were shown in Fig. 3. The pure melamine foam has a three-dimensional interconnected network structure (Fig. 3(a)) with a smooth surface. The average pore size of the pure melamine foam was 133 ± 3 μm. When the melamine foam was coated with g-C_3N_4/Bi_2S_3, the average pore size decreased to 103 μm, indicating a uniform coating of g-C_3N_4/Bi_2S_3 on the melamine foam (Fig. 3(b) and (c)). The SEM images suggest that the g-C_3N_4/Bi_2S_3 particles have roughened the foam surface, creating micro- and nano-protrusions on its smooth network structure. These protrusions mimic the lotus leaf effect, resulting in the g-C_3N_4/Bi_2S_3 foams superhydrophobic properties.

XPS analysis

The XPS of the g-C_3N_4/Bi_2S_3 foam is shown in Fig. 4. The survey scan XPS (Fig. 4(a)) reveal the oxidation states and surface compositions of g-C_3N_4/Bi_2S_3 foam. The narrow scan XPS for each element were fitted using the Voigt function. The two components present in the C 1s XPS spectrum of g-C_3N_4/Bi_2S_3 foam (Fig. 4(b)), correspond to C=C bond within the graphitic structure (284.5 eV) and N=C(N)$_2$ groups (287.6 eV). Fig. 4(c) reveals N 1s spectra of chemically distinct N species with binding energies at 398.0, 399.9, and 400.2 eV, corresponding to C=N–C bonds, N–(C)$_3$ groups, and surface uncondensed bridging N atoms with C–N–H functional groups.[22] In Fig. 4(d), the Bi $4f_{5/2}$ and Bi $4f_{7/2}$ peaks exhibit a typical spin–orbit doublet splitting of 5.4 eV, appearing at 163.6 and 158.3 eV, respectively, closely matching the standard Bi^{3+} peaks in Bi_2S_3. The peak located between Bi $4f_{5/2}$ and Bi $4f_{7/2}$ is assigned to S $2p_{3/2}$ (161.0 eV). The peaks at 163.2 and 158.1 eV can be attributed to the Bi^0 state of metallic Bi 4f.[23–25] Literature reports indicate that the pure melamine foams comprise only the presence of C, N, and O elements.[26] So, it can be inferred that g-C_3N_4/Bi_2S_3 is successfully coated on the melamine foam.

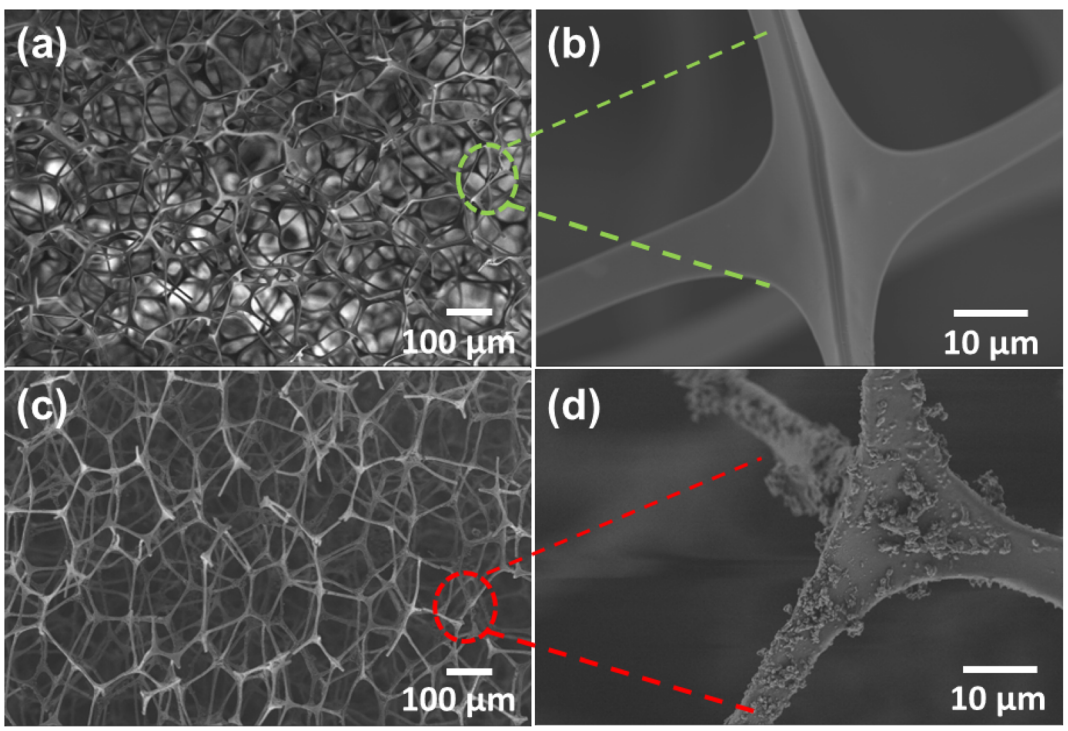

Fig. 3 FESEM images of (a and b) pure melamine foam and (c and d) g-C_3N_4/Bi_2S_3 coated melamine foam at different magnifications.

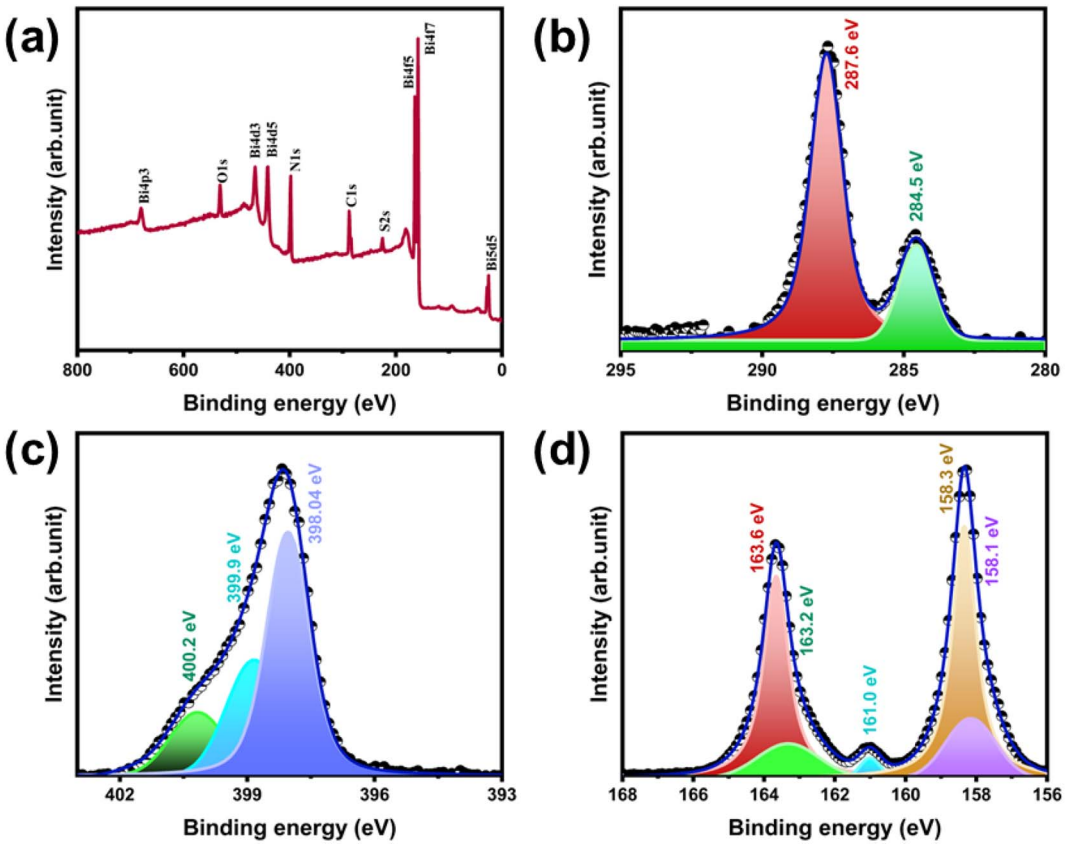

Fig. 4 XPS (a) survey scan of g-C_3N_4/Bi_2S_3 foam. (b)–(d) Narrow scan XPS of g-C_3N_4/Bi_2S_3 foam: (b) C 1s and (c) N 1s and (d) Bi 4f.

TGA and FTIR analysis

Fig. 5(a) presents the thermal degradation analysis of pure melamine foam and g-C_3N_4/Bi_2S_3 foam. The mass loss of both melamine and g-C_3N_4/Bi_2S_3 foams can be categorized into four temperature ranges: (a) zone 1: 35–150 °C, (b) zone 2: 170–365 °C, (c) zone 3: 370–415 °C and zone 4: above 415 °C. The mass loss in zone 1 was attributed to the evaporation of adsorbed thin layer of water on the foam surface, the mass loss in zone 2 was mostly due to the elimination of formaldehyde from the ether bridges, the mass loss in zone 3 was because of the breakdown of the methylene linkages and zone 4 was mainly due to the thermal decomposition of the triazine ring.[27,28] The TGA of the g-C_3N_4/Bi_2S_3 foam shows a slight variation, attributed to the incorporation of g-C_3N_4/Bi_2S_3 within the melamine skeleton. To determine if any chemical changes occur in the g-C_3N_4/Bi_2S_3 foam after oil absorption, FTIR spectra of the g-C_3N_4/Bi_2S_3 foams were obtained before and after oil absorption. The results, as shown in Fig. 5(b), indicated no significant changes

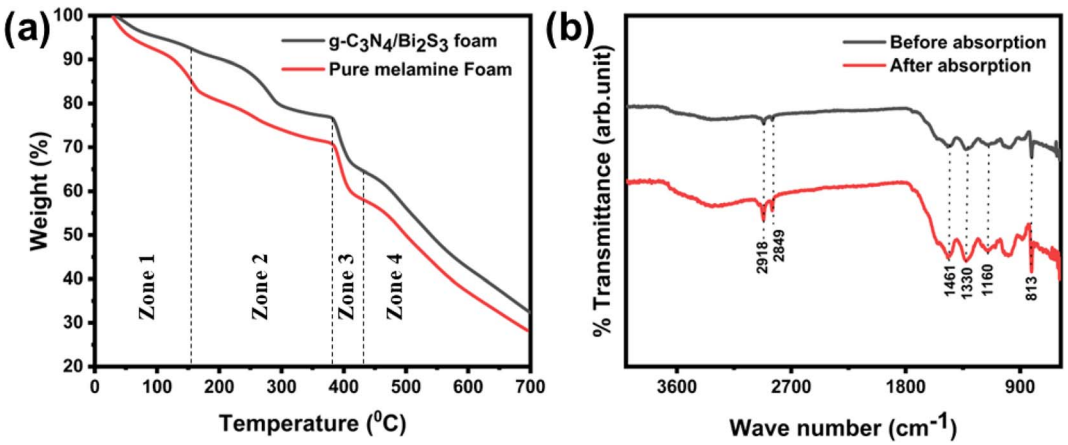

Fig. 5 (a) TGA for the g-C_3N_4/Bi_2S_3 foam and pure melamine foam. (b) FTIR spectra of g-C_3N_4/Bi_2S_3 foam before and after absorption.

in the spectra. The broad peak observed between 3250–3600 cm^{-1} indicates O–H asymmetric stretching modes of secondary and primary amines, in addition to the stretching vibrations of the O–H bond from absorbed water molecules and their intermolecular hydrogen-bonding interactions. The bands within the 1200–1600 cm^{-1} range are characteristic of aromatic carbon nitride heterocycles. The band near 813 cm^{-1} corresponds to the stretching vibrations of the triazine ring, and other characteristic peaks at 1755 cm^{-1}, 2849 cm^{-1} and 2919 cm^{-1} corresponding to C=O and symmetric and asymmetric stretching vibrations of methylene.[27–32]

Wettability study

The wettability of an adsorbent is determined by its surface energy and surface morphology.[33] WCA measurements of Bi_2S_3 on a glass slide demonstrated its hydrophobicity, with a WCA of 131.3 ± 3°. The binary composite with Bi_2S_3 and 250 mg of g-C_3N_4 showed better oleophilic nature compared to other composite materials, with a WCA of 130.1 ± 1°. The melamine foam coated with g-C_3N_4/Bi_2S_3 composite and dopamine hydrochloride achieved a superhydrophobic surface, retaining water droplets at a WCA of 159.5 ± 1° (as shown in Fig. 6(a) and (b)). For comparison, the WCA for unmodified melamine foam and pure g-C_3N_4 was measured at 0°, indicating hydrophilic behavior. Fig. 6(c) illustrates this, where a 6 μl water droplet rapidly penetrates the unmodified melamine foam, demonstrating superhydrophilicity.

In this study, the WCA was measured before and after coating the dopamine hydrochloride on the g-C_3N_4/Bi_2S_3 foam to look for any variations in the WCA during the coating process. The results showed negligible variation in the WCA (WCA before: 160.1 ± 1° and WCA after: 159.5 ± 1°). Reported studies shows that materials like polydopamine, polyvinylidene fluoride (PVDF), and polydimethylsiloxane (PDMS) enhance particle adherence on similar foams.[34–38] Based on the analysis, the unique structure and surface chemical composition create the essential conditions for the development of a superwetting material. On the other hand, by the dip coating method, the foam surface was uniformly covered by g-C_3N_4/Bi_2S_3, resulting in the formation of a hierarchical micro–nano structure. The combination of adsorbent with a rough hierarchical structure with low surface energy leads to superhydrophobic properties on melamine foam.[39] The surface free energy of oil, which typically ranges from 20 to 60 mN m^{-1}, is generally lower than that of water (72 mN m^{-1}). According to Young's equation, a lower surface tension increases the tendency of a liquid to spread over a solid surface.[40] The g-C_3N_4/Bi_2S_3 foam showed superhydrophobic nature with super oleophilicity, because water has greater surface tension than oils. The g-C_3N_4/Bi_2S_3 foam exhibited superhydrophobic properties and super oleophilicity due to the lower surface tension of oils compared to water. The WCA studies on PDA suggest that the separation efficiency of the superhydrophobic g-C_3N_4/Bi_2S_3 foam is a synergistic result of the micro-/nano protrusions and the hierarchical three-dimensional porous structure in conjunction with the PDA coating.

The sliding angles of g-C_3N_4/Bi_2S_3 foam with PDA coating and melamine foam with PDA coating were measured. The sliding angle measured for g-C_3N_4/Bi_2S_3 foam was < 10° and that for melamine foam with PDA coating was > 20°. A sliding angle < 10° signifies that the superhydrophobic surface exhibits

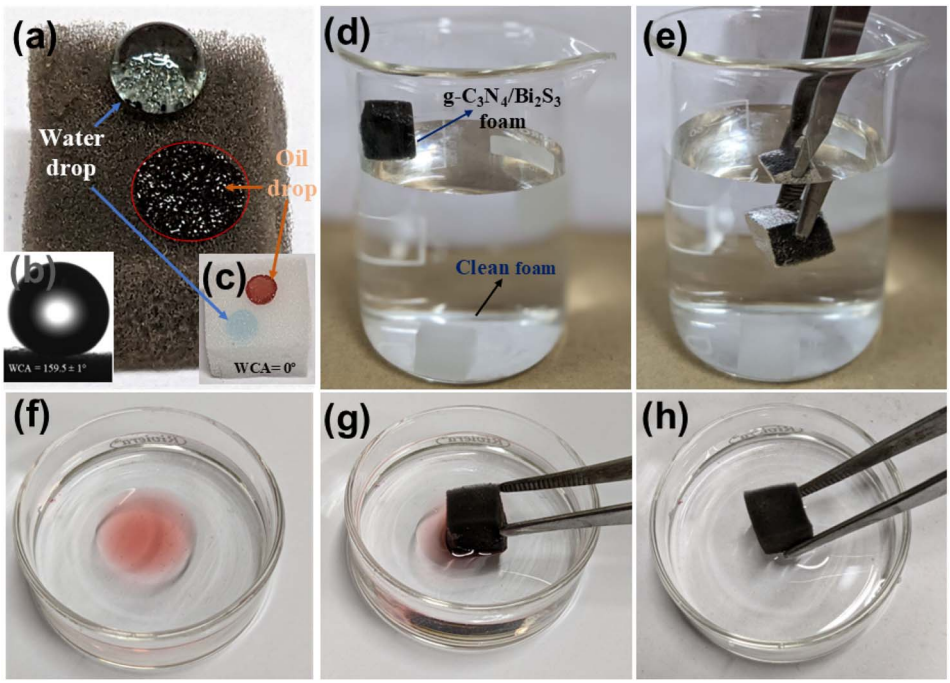

Fig. 6 (a) The water and oil droplets on the g-C_3N_4/Bi_2S_3 foam surface. Inset (b): WCA of g-C_3N_4/Bi_2S_3 foam; inset (c): water and oil droplets on a pure melamine foam. (d and e) photographs of the g-C_3N_4/Bi_2S_3 foam and a pure melamine foam immersed in water. (f–h) Present sequential photographs demonstrating the oil removal process from water using the g-C_3N_4/Bi_2S_3 foam.

self-cleaning properties and is suitable for efficient oil/water separation.[41]

Oil/water separation performance of the g-C_3N_4/Bi_2S_3 foam

The superhydrophobic nature of a material can be achieved by attaining appropriate surface energy, surface roughness, or specific morphology. Incorporating hydrophobic materials into a system can alter surface wettability, resulting in superhydrophobicity with a water contact angle (WCA) greater than 150°. Materials such as foams are inherently super hydrophilic due to their porous nature, high surface roughness, and large surface area, which make them effective absorbers of liquids and oils.[42,43] When hydrophobic materials are incorporated into the skeleton, the super hydrophilic property of the foam is converted to superhydrophobicity due to the change in surface wettability. The wettability of the surface is influenced by three different interfacial forces: solid–liquid, solid–vapor, and interfacial tensions. This transition from super hydrophilic to superhydrophobic absorption properties can be utilized for applications in oil/water separation and absorbing organic solvents. Numerous studies have reported the use of commercially available foams incorporated with hydrophobic nanomaterials for oil/water separation.[43,44]

In this study, the hydrophobic g-C_3N_4/Bi_2S_3 binary composite was incorporated onto the foam surface to alter the surface roughness, thereby the surface wettability. A simple dip coating and drying were used for the preparation of g-C_3N_4/Bi_2S_3 foam. The particle loading percentage was obtained using eqn (1),

$$\text{Particle loading}\% = \frac{W_{GB} - W_M}{W_M} \times 100\% \quad (1)$$

where W_{GB} and W_M are the weights of g-C_3N_4/Bi_2S_3 loaded foam, and pure melamine foam respectively.[45] The physical interaction holds the g-C_3N_4/Bi_2S_3 particles on the melamine foam surface. *i.e.*, the g-C_3N_4/Bi_2S_3 particles adhere as a result of the strong van der Waals force of attraction between the foam surface and g-C_3N_4/Bi_2S_3 particles.[45,46] The g-C_3N_4/Bi_2S_3 binary composites were incorporated into the melamine foam using a simple dip-coating technique, followed by manual squeezing of the foam. The loading percentage of the g-C_3N_4/Bi_2S_3 foam was determined using eqn (1), by comparing the weight of the g-C_3N_4/Bi_2S_3 foam before and after g-C_3N_4/Bi_2S_3 binary composite incorporation. At lower nanoparticle loading percentages, the foam readily absorbs the water droplet. It was observed that at approximately 44.4% g-C_3N_4/Bi_2S_3 nanocomposite particles loading in the foam, the water droplet formed a spherical shape, with a WCA of 159.5 ± 1° (see ESI document Fig. S2 and S3†). Further increases in nanoparticle loading led to higher WCA values; however, excessive loading eventually compromised the absorption capacity of the foam due to pore blockage by the nanoparticles. Fig. 6 illustrates g-C_3N_4/Bi_2S_3 foam that exhibits superhydrophobic properties, holding water droplets on its surface with a water contact angle (WCA) of 159.5 ± 1°. Additionally, the foam demonstrates superoleophilic characteristics, absorbing oil with a contact angle (CA) of 0°. The inset of Fig. 6(c) illustrates the appearance of water (blue color) and oil (red color) droplets on a blank melamine foam absorbed by the foam surface. Fig. 6(d) presents a photograph showing a clean melamine foam (white color) and the g-C_3N_4/Bi_2S_3 foam (black color) placed in water. The contact hysteresis of the g-C_3N_4/Bi_2S_3 foam was determined by measuring the dynamic contact angle by tilting the sample stage. The contact hysteresis, calculated as the difference between the advancing and receding contact angles, was found to be 1.5 ± 1.3°. This low value of contact hysteresis indicates that water droplets easily slide off the foam surface. The bare melamine foam absorbs water and settles down at the bottom of the beaker and the g-C_3N_4/Bi_2S_3 foam floats on the surface of the water. When an external force was applied to dip the g-C_3N_4/Bi_2S_3 foam into water and then released, it rebounded without absorbing any water (Fig. 6(e)). While immersing g-C_3N_4/Bi_2S_3 foam into the water, the g-C_3N_4/Bi_2S_3 foam exhibited a shiny silver-colored appearance due to the air layer trapped between the foam surface and water, attributed to its high surface roughness. This phenomenon is consistent with the characteristics of a non-wetting Cassie–

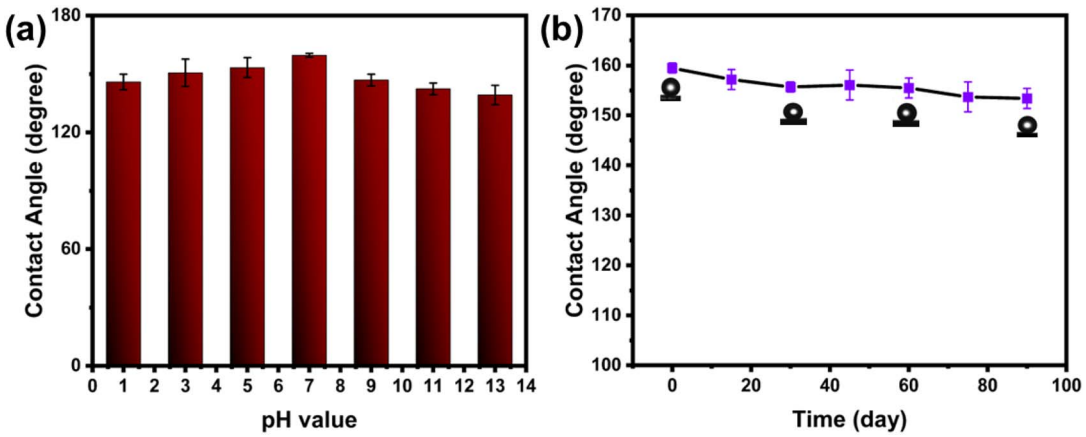

Fig. 7 (a) Stability test of the g-C_3N_4/Bi_2S_3 foam after 24 h in the solutions with different pH values. (b) Variation in the WCA of g-C_3N_4/Bi_2S_3 foam with exposure to air over a period of 0 to 90 days.

Baxter surface.[47] Fig. 6(f)–(h) demonstrates the separation of oil from water using the prepared g-C_3N_4/Bi_2S_3 foam. The g-C_3N_4/Bi_2S_3 foam absorbed oil within 3–6 s upon contact with oily water, thereby effectively removing oil from water. Thus, the g-C_3N_4/Bi_2S_3 foam has demonstrated an effective capacity for absorbing oils.

To assess the durability of the g-C_3N_4/Bi_2S_3 foam in a corrosive environment, it was immersed in aqueous solutions with pH values of 1, 3, 5, 7, 9, 11, and 13. After a 24 h period, the g-C_3N_4/Bi_2S_3 foam remained floating on the surface of these solutions. After the corrosion test, the WCAs were measured to detect any variations in the foam's contact angle, as depicted in Fig. 7(a). The results indicated a minor decrease in WCA values; however, the foams retained their stable hydrophobic characteristics. This analysis demonstrates that the g-C_3N_4/Bi_2S_3 foam exhibits substantial corrosion resistance in corrosive environments. Moreover, the variation in the WCA of g-C_3N_4/Bi_2S_3 foam upon exposure to air over 0–90 days is illustrated in Fig. 7(b). After 90 days in the air, the WCA of g-C_3N_4/Bi_2S_3 foam exhibited only a slight decrease from its initial value of 159.5 ± 1° to 153.4 ± 2°, indicating superior long-term durability. This stable superhydrophobicity of g-C_3N_4/Bi_2S_3 foam is attributed to the satisfactory adhesion of PDA and the excellent chemical stability of the g-C_3N_4/Bi_2S_3 binary nanocomposite, which together maintain the presence of low surface energy and rough structures on the melamine foam substrate. Therefore, the superhydrophobic g-C_3N_4/Bi_2S_3 foam is a viable candidate for practical applications.

The superhydrophobic and superoleophilic characteristics of the g-C_3N_4/Bi_2S_3 foams were tested using various organic solvents and oils. Organic solvents like ethanol, methanol, toluene, DMF, acetone, and chloroform were used to study the absorption capacity of g-C_3N_4/Bi_2S_3 foam. Fig. 8(a) illustrates the absorption capacity of the g-C_3N_4/Bi_2S_3 foam for these organic solvents and oils. The absorption capacity of the organic solvents and oils is influenced by their viscosity, density, and surface tension. The absorption capacities for oils such as olive oil, pump oil, engine oil, and crude oil were also used for oil/water separation studies. The maximum absorption capacity was observed for engine oil, ~89 times the original weight of the foam.

Absorption capacity and recyclability of the g-C_3N_4/Bi_2S_3 foam

A suitable absorber should possess high absorption capacity and recyclability. The absorption capacity and recyclability of the g-C_3N_4/Bi_2S_3 foam were evaluated using two methods: (i) manual squeezing and (ii) one-step continuous separation. In the manual squeezing method, the absorption recyclability of the g-C_3N_4/Bi_2S_3 foam was tested with various organic solvents and oils. It was observed that effective separation could be achieved for up to 20 cycles without any material loss, as depicted in Fig. 8(b). The g-C_3N_4/Bi_2S_3 foam showed excellent absorption recyclability for organic solvents and oils. The manual squeezing method involves simply immersing and squeezing the g-C_3N_4/Bi_2S_3 foam in the oil or organic solvent to collect the absorbed liquid, making it an eco-friendly and time-saving alternative to heating methods or burn-off techniques. The absorption capacity of the foam was determined by the weight gain ratio, as calculated from eqn (2).[48]

$$\text{Absorption capacity} = \frac{W_2 - W_1}{W_1} \quad (2)$$

where W_1 and W_2 denote the weights of the g-C_3N_4/Bi_2S_3 foam before and after the absorption of oils or organic solvents, respectively. The g-C_3N_4/Bi_2S_3 foam demonstrated significant absorption capacity for a variety of oils and organic solvents, with values ranging from 31 to 89 times its initial weight. The foam retained its superhydrophobic properties for up to 5–6 cycles, after which the WCA decreased to approximately 142°. However, the overall performance remained unaffected. For oil absorption specifically, the capacity decreased to around 12 times its original weight after the first cycle, as illustrated in Fig. 8(b). This reduction was attributed to the incomplete removal of residual oil by manual squeezing. Therefore, the method of oil/water separation *via* manual squeezing significantly impacts the efficiency of the g-C_3N_4/Bi_2S_3 foam. In contrast, when used for the

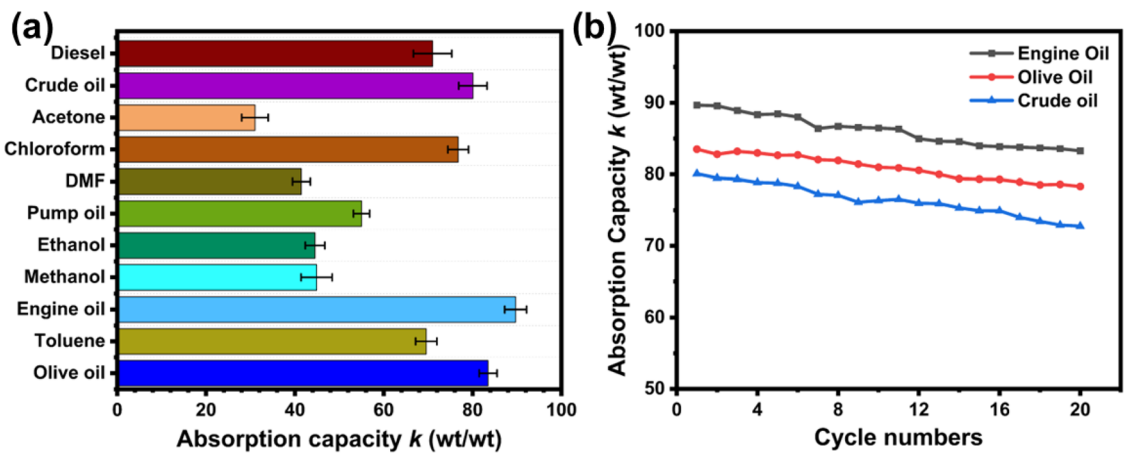

Fig. 8 (a) The absorption capacity of g-C_3N_4/Bi_2S_3 foam with different organic solvents and oils. (b) Recyclability of g-C_3N_4/Bi_2S_3 foam absorption using manual squeezing for oil recovery.

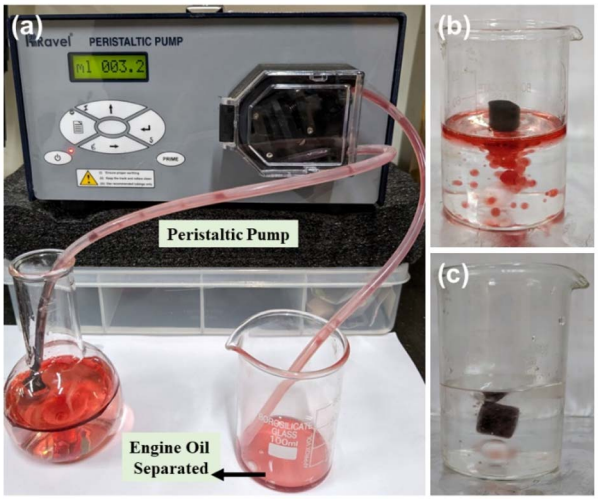

Fig. 9 The separation of oil from water using the g-C_3N_4/Bi_2S_3 foam by: (a) continuous separation facilitated by a peristaltic pump, and (b and c) continuous stirring of oil in water.

absorption of organic solvents, no significant change in saturation absorption capacity was observed, indicating promising recyclability of the g-C_3N_4/Bi_2S_3 foam.

To investigate the maximum separation efficiency of oils using the g-C_3N_4/Bi_2S_3 foam, the second separation method was employed with a peristaltic pump (Ravel Hiteks Pvt. Ltd, RHP100). Fig. 9(a) demonstrates the oil/water separation by the g-C_3N_4/Bi_2S_3 foam using the peristaltic pump. The g-C_3N_4/Bi_2S_3 foam effectively removed 25 ml of engine oil from water without any loss of g-C_3N_4/Bi_2S_3 nanocomposite from the melamine foam. This one-step separation method highlights the high absorption capacity of the g-C_3N_4/Bi_2S_3 foam for engine oil in water. The study confirms the efficiency of the g-C_3N_4/Bi_2S_3 foam in extracting a substantial amount of oil from water. Furthermore, the superhydrophobic g-C_3N_4/Bi_2S_3 foam efficiency was evaluated under dynamic conditions by continuously stirring engine oil in water at 600 rpm. The selective separation of engine oil from water under continuous stirring is depicted in Fig. 9(b) and (c).

To evaluate the separation efficiency of the g-C_3N_4/Bi_2S_3 foam, a surfactant-stabilized oil/water emulsion was prepared and utilized. Specifically, a toluene-in-water emulsion was created by vigorous stirring for 2 h with the addition of sodium dodecyl sulfate. The emulsion was prepared using a mixture of water and toluene (1 : 1). The prepared emulsion was processed through the g-C_3N_4/Bi_2S_3 foam, resulting in a clear and transparent filtrate. Optical imaging of the filtrate indicated the

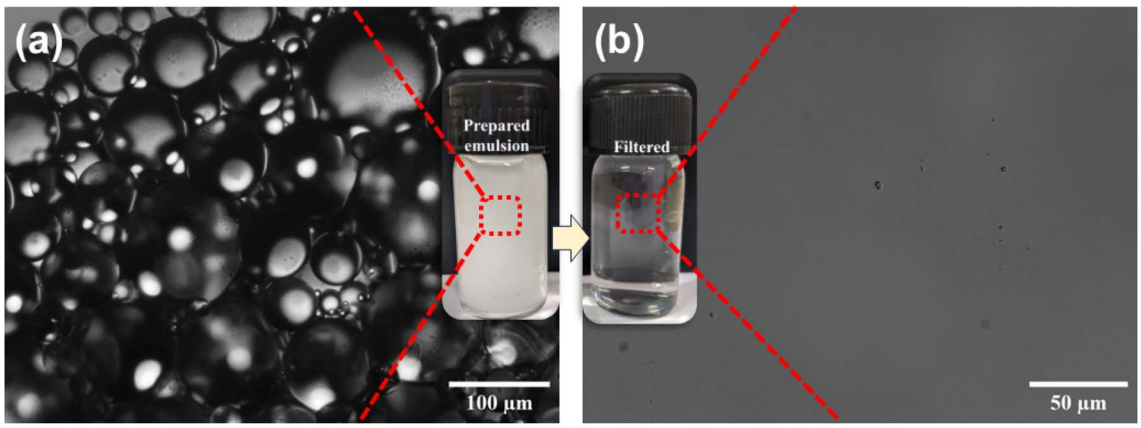

Fig. 10 Photograph of the prepared oil-in-water emulsion (a) before and (b) after separation.

Table 1 Comparative analysis of g-C_3N_4/Bi_2S_3 foam and nanomaterial-based adsorbents in oil/water separation studies

Sorbents	WCA (°)	Maximum absorption capacity (wt/wt)	Reference
CNT–PU sponge	158	35	48
Nanodiamond–PU	143 ± 2	59.26	49
Reduced graphene oxide foam	—	5–40	50
Silylated wood sponge	151	16–41	51
PDVB–PDMS	153	78	52
Carbon soot sponge	144	80	53
SiO_2/GO–PU sponge	145	80–180	54
PVP-melamine sponge	135	49	55
PPy–PA PU sponge	140	22–62	56
USTC-6-GO sponge	132	12–43	57
Acylated melamine sponge	140	66.6–168.2	58
g-C_3N_4/Bi_2S_3 foam	159.5 ± 1	31–89.7	This work

absence of noticeable droplets, as shown in Fig. 10. This observation suggests that the stability of the emulsion is significantly disrupted due to the superhydrophobic and superoleophilic properties of the g-C_3N_4/Bi_2S_3 foam, leading to demulsification. The extensive contact surface of the superhydrophobic foam, combined with the intermolecular forces between the foam and the nonpolar oil-in-water droplets, facilitates the emulsion separation. This study confirms that the g-C_3N_4/Bi_2S_3 foam is highly effective for emulsion separation.

Table 1 provides a comparative analysis of nanoparticle-embedded adsorbents reported for oil/water separation, including the current study. In this study, the g-C_3N_4/Bi_2S_3 foam, when compared to other adsorbents, exhibits superior absorption capacity. The cost-effective, simple, and scalable synthesis of g-C_3N_4/Bi_2S_3 makes the foam a promising adsorbent material for oil/water separation applications.

Conclusions

In this study, g-C_3N_4/Bi_2S_3 foam adsorbent was synthesized using a simple dip coating method. This approach involves the incorporation of hydrothermally-synthesized g-C_3N_4/Bi_2S_3 into a melamine foam. The resulting g-C_3N_4/Bi_2S_3 foam exhibited unique surface morphology and chemical composition, leading to superhydrophobic and superoleophilic characteristics. Experimental findings revealed that the g-C_3N_4/Bi_2S_3 foam showed the ability to separate organic solvents and oils from water. The manual squeezing and one-step continuous separation methods demonstrate a superior absorption capacity for the g-C_3N_4/Bi_2S_3 foam compared to previous reports. Additionally, the g-C_3N_4/Bi_2S_3 foam exhibits exceptional separation efficiency for oil-in-water emulsions. Experimental findings suggest that this g-C_3N_4/Bi_2S_3 foam is a promising solution for oily wastewater treatment.

Data availability

The data supporting this article have been included as part of the ESI.† See ESI† for XRD, SEM, photographs and oil removal capacity of prepared samples (Fig. S1–S5 and Videos S6 and S7†).

Conflicts of interest

There are no conflicts to declare.

Acknowledgements

The authors acknowledge the Department of Physics, National Institute of Technology Calicut, for XRD (FIST, Grant No. SR/FST/PSI-113/2019) and FTIR facilities. The authors also thank to optofluidics and interface science laboratory for optical imaging and contact angle measurements of the samples. Financial support from the University Grants Commission (UGC), New Delhi, India is also gratefully acknowledged.

References

1 Z. Asif, Z. Chen, C. An and J. Dong, *J. Mar. Sci. Eng.*, 2022, **10**, 762.
2 D. R. E. Ewim, O. F. Orikpete, T. O. Scott, C. N. Onyebuchi, A. O. Onukogu, C. G. Uzougbo and C. Onunka, *Bull. Natl. Res. Cent.*, 2023, **47**, 116.
3 R. M. Abou Samra and R. R. Ali, *Mar. Pollut. Bull.*, 2024, **198**, 115887.
4 B. V. Malozyomov, N. V. Martyushev, V. V. Kukartsev, V. S. Tynchenko, V. V. Bukhtoyarov, X. Wu, Y. A. Tyncheko and V. A. Kukartsev, *Energies*, 2023, **16**, 4907.
5 K. V. Udayakumar, P. M. Gore and B. Kandasubramanian, *Chem. Eng. J. Adv.*, 2021, **5**, 100076.
6 N. Y. Abu-Thabit, O. J. Uwaezuoke and M. H. Abu Elella, *Chemosphere*, 2022, **294**, 133644.
7 H. Wang, Q. Zhao, K. Zhang, F. Wang, J. Zhi and C.-X. Shan, *Langmuir*, 2022, **38**, 11304–11313.
8 M. Talukdar, S. K. Behera, K. Bhattacharya and P. Deb, *Appl. Surf. Sci.*, 2019, **473**, 275–281.
9 D. Liu, S. Wang, T. Wu and Y. Li, *Nanomaterials*, 2021, **11**, 3344.
10 M. Ezazi and M. M. Quazi, *Membranes*, 2023, **13**, 677.
11 Y. Xin, B. Qi, X. Wu, C. Yang and B. Li, *Colloid Interface Sci. Commun.*, 2024, **59**, 100772.
12 S. Wang, L. Wang, H. Cong, R. Wang, J. Yang, X. Li, Y. Zhao and H. Wang, *J. Environ. Chem. Eng.*, 2022, **10**, 108189.
13 R. Yue and Md. Saifur Rahaman, *J. Colloid Interface Sci.*, 2022, **608**, 1960–1972.
14 H. Mao, Q. Zhang, F. Cheng, Z. Feng, Y. Hua, S. Zuo, A. Cui and C. Yao, *Ind. Eng. Chem. Res.*, 2022, **61**, 8895–8907.
15 S. Mir, A. Naderifar, A. Rahidi and M. Alaei, *Environ. Sci. Pollut. Res.*, 2022, **29**, 66888–66901.
16 L. Li, C. Luo, X. Chen, N. Chu, L. Li, M. Chao and L. Yan, *Adv. Funct. Mater.*, 2023, **33**, 2213974.
17 Z. Chen and M. Cao, *Mater. Res. Bull.*, 2011, **46**, 555–562.
18 Y. Xiao, H. Cao, K. Liu, S. Zhang and V. Chernow, *Nanotechnology*, 2010, **21**, 145601.
19 R. C. Pawar, S. Kang, S. H. Ahn and C. S. Lee, *RSC Adv.*, 2015, **5**, 24281–24292.
20 B. Zhu, P. Xia, W. Ho and J. Yu, *Appl. Surf. Sci.*, 2015, **344**, 188–195.
21 Y.-J. Yuan, Z. Shen, S. Wu, Y. Su, L. Pei, Z. Ji, M. Ding, W. Bai, Y. Chen, Z.-T. Yu and Z. Zou, *Appl. Catal., B*, 2019, **246**, 120–128.
22 B. Zhang, X. Hu, E. Liu and J. Fan, *Chin. J. Catal.*, 2021, **42**, 1519–1529.
23 E. Miniach and G. Gryglewicz, *J. Mater. Sci.*, 2018, **53**, 16511–16523.
24 S. Singh, R. K. Sahoo, N. M. Shinde, J. M. Yun, R. S. Mane and K. H. Kim, *Energies*, 2019, **12**, 3320.
25 H. Shen, Z. Shao, Q. Zhao, M. Jin, C. Shen, M. Deng, G. Zhong, F. Huang, H. Zhu, F. Chen and Z. Luo, *J. Colloid Interface Sci.*, 2020, **573**, 115–122.
26 C. Yan, Y. Luo, W. Zhang, Z. Zhu, P. Li, N. Li, Y. Chen and T. Jin, *J. Appl. Polym. Sci.*, 2022, **139**, 51992.

27 Y. Tang, D. Li, D. Ao, S. Li and X. Zu, *J. Mater. Sci.: Mater. Electron.*, 2018, **29**, 13643–13652.
28 Y. Liu, Z. Chen, J. Zhang, S. Ai and H. Tang, *J. Porous Mater.*, 2019, **26**, 1305–1312.
29 J. Arumugam, A. Dhayal Raj and A. Albert Irudayaraj, *J. Mater. Sci.: Mater. Electron.*, 2017, **28**, 3487–3494.
30 S. Pareek, M. Sharma, S. Lal and J. K. Quamara, *J. Mater. Sci.: Mater. Electron.*, 2018, **29**, 13043–13051.
31 J. Yin, Z. Wu, M. Fang, Y. Xu, W. Zhu and C. Li, *J. Chin. Biochem. Soc.*, 2018, **65**, 1044–1052.
32 T. Zhao, X. Zhu, Y. Huang and Z. Wang, *RSC Adv.*, 2021, **11**, 9788–9796.
33 H. Yao, Z. Xie, C. Huang, Q. Yuan and Z. Yu, *Constr. Build. Mater.*, 2021, **299**, 124255.
34 L. Lefebvre, J. Kelber, L. Jierry, V. Ritleng and D. Edouard, *J. Environ. Chem. Eng.*, 2017, **5**, 79–85.
35 K. Y. Eum, I. Phiri, J. W. Kim, W. S. Choi, J. M. Ko and H. Jung, *Korean J. Chem. Eng.*, 2019, **36**, 1313–1320.
36 Lipika and A. K. Singh, *Cleaner Mater.*, 2022, **6**, 100136.
37 R. Jiang, T. Bian, X. Zheng, Y. Cui, Y. Zhang, M. Li and Z. Li, *Mater. Chem. Phys.*, 2021, **273**, 125080.
38 W. Liu, X. Huang, K. Peng, Y. Xiong, J. Zhang, L. Lu, J. Liu and S. Li, *Surf. Coat. Technol.*, 2021, **406**, 126743.
39 X. Wang and Q. Zhang, *Powder Technol.*, 2020, **371**, 55–63.
40 K.-Y. Law, *Pure Appl. Chem.*, 2015, **87**, 759–765.
41 S. Barthwal, S. Barthwal, B. Singh and N. Bahadur Singh, *Colloids Surf., A*, 2020, **597**, 124776.
42 Y. Guan, F. Cheng and Z. Pan, *Polymers*, 2019, **11**, 806.
43 N. Y. Abu-Thabit, O. J. Uwaezuoke and M. H. Abu Elella, *Chemosphere*, 2022, **294**, 133644.
44 Z. Chu, Y. Feng and S. Seeger, *Angew. Chem., Int. Ed.*, 2015, **54**, 2328–2338.
45 R. Panickar, C. B. Sobhan and S. Chakravorti, *Langmuir*, 2021, **37**, 12501–12511.
46 E. K. Sam, J. Liu and X. Lv, *Ind. Eng. Chem. Res.*, 2021, **60**, 2353–2364.
47 X. Zhang, W. Zhu, G. He, P. Zhang, Z. Zhang and I. P. Parkin, *J. Mater. Chem. A*, 2016, **4**, 14180–14186.
48 H. Wang, E. Wang, Z. Liu, D. Gao, R. Yuan, L. Sun and Y. Zhu, *J. Mater. Chem. A*, 2015, **3**, 266–273.
49 N. Cao, B. Yang, A. Barras, S. Szunerits and R. Boukherroub, *Chem. Eng. J.*, 2017, **307**, 319–325.
50 Z. Niu, J. Chen, H. H. Hng, J. Ma and X. Chen, *Adv. Mater.*, 2012, **24**, 4144–4150.
51 H. Guan, Z. Cheng and X. Wang, *ACS Nano*, 2018, **12**, 10365–10373.
52 J. Zhang, R. Chen, J. Liu, Q. Liu, J. Yu, H. Zhang, X. Jing, P. Liu and J. Wang, *Chemosphere*, 2020, **239**, 124793.
53 Y. Gao, Y. S. Zhou, W. Xiong, M. Wang, L. Fan, H. Rabiee-Golgir, L. Jiang, W. Hou, X. Huang, L. Jiang, J.-F. Silvain and Y. F. Lu, *ACS Appl. Mater. Interfaces*, 2014, **6**, 5924–5929.
54 X. Lü, Z. Cui, W. Wei, J. Xie, L. Jiang, J. Huang and J. Liu, *Chem. Eng. J.*, 2016, **284**, 478–486.
55 Z. Lei, G. Zhang, Y. Deng and C. Wang, *Appl. Surf. Sci.*, 2017, **416**, 798–804.
56 M. Khosravi and S. Azizian, *ACS Appl. Mater. Interfaces*, 2015, **7**, 25326–25333.
57 Z.-R. Jiang, J. Ge, Y.-X. Zhou, Z. U. Wang, D. Chen, S.-H. Yu and H.-L. Jiang, *NPG Asia Mater.*, 2016, **8**, e253.
58 O. Oribayo, Q. Pan, X. Feng and G. L. Rempel, *AIChE J.*, 2017, **63**, 4090–4102.